Available online at www.sciencedirect.com

ScienceDirect

Ceramics International 40 (2014) 3495–3502

CERAMICS INTERNATIONAL

www.elsevier.com/locate/ceramint

Highly efficient visible light-driven Ag/AgBr/ZnO composite photocatalyst for degrading Rhodamine B

Lei Shi[b], Lin Liang[a,c], Jun Ma[a], Yanan Meng[b], Shifa Zhong[b], Fangxiao Wang[b], Jianmin Sun[a,b,*]

[a]State Key Laboratory of Urban Water Resource and Environment, Harbin Institute of Technology, Harbin 150080, China
[b]The Academy of Fundamental and Interdisciplinary Science, Harbin Institute of Technology, Harbin 150080, China
[c]School of Life Science and Technology, Harbin Institute of Technology, Harbin 150080, China

Received 25 July 2013; received in revised form 17 September 2013; accepted 17 September 2013
Available online 28 September 2013

Abstract

In this paper, Ag/AgBr/ZnO composites have been successfully synthesized by two steps of deposition–precipitation method, then followed by reduction under visible light irradiation. The results of X-ray diffraction and X-ray photoelectron spectroscopy confirmed Ag/AgBr nanoparticles were loaded on ZnO support. The transmission electron microscopy showed Ag/AgBr nanoparticles with small sizes of 5 nm were well attached on the surface of ZnO, which made Ag/AgBr/ZnO composites display strong absorption in the visible light range. Ag/AgBr/ZnO composites showed much better photocatalytic activities for degradation of Rhodamine B dye under visible light than pure ZnO. The enhanced photocatalytic activity may be ascribed to the synergetic effects including enhanced visible light absorption, narrowed band gap and effective separation of photogenerated electron–hole pairs. In addition, catalytic repetitive tests showed that Ag/AgBr/ZnO composite maintained good stability and the activity decreased slightly after 10 cycles. The possible mechanism was tentatively proposed based on the photoluminescence spectra and the reaction effects by adding the radical scavengers.

Keywords: Ag/AgBr/ZnO composites; Photocatalyst; Visible light; RhB dye

1. Introduction

Over the past several decades, environmental contaminations caused by wastewater have become a serious problem. Dye wastewater especially coming from textile industries, due to toxic and mostly nonbiodegradable, was hard to be treated. Some traditional methods such as adsorption, membrane filtration and chemical precipitation have been applied for removing the dyes [1–3]. In recent years, photocatalysis technology is considered as alternative and efficient method for degrading various hazardous contaminants, moreover, many semiconductors such as TiO_2 [4], ZnO [5], Co_3O_4 [6], CuO [7], CdS [8] etc. are reported to be effective photocatalysts. ZnO as a good photocatalyst, has been attracting much attention in the past decades owing to its high activity in the ultraviolet range, low cost, thermal and chemical stability and environmentally friendly features [9]. However, the large band gap of 3.2 eV makes ZnO only collect ultraviolet light, which only accounts for a small fraction 4% of the solar spectrum. Moreover, the low separating efficiency of the photogenerated electron–hole pairs also makes its photocatalytic ability not high enough. The two problems both restrict the photocatalytic degradation efficiency of the pollutants and its broader applications. In order to solve these drawbacks, a lot of methods such as metal ion doping [10], non-metal doping [11], noble metal deposition [12], coupling with composite semiconductors [13], photosensitive material modification [14], and conjugated polymer modification [15] have been applied for improving the photocatalytic activity of ZnO.

Recently, efficient Ag/AgX (X=Cl, Br and I) photocatalysts have been developed [16–18]. Due to the presence of noble metal Ag, Ag/AgX nanoparticles possess strong absorption in the visible light range and can effectively separate photogenerated

*Corresponding author at: State Key Laboratory of Urban Water Resource and Environment, Harbin Institute of Technology, Harbin 150080, China. Tel.: +86 451 86403715.
E-mail address: sunjm@hit.edu.cn (J. Sun).

0272-8842/$ - see front matter © 2013 Elsevier Ltd and Techna Group S.r.l. All rights reserved.
http://dx.doi.org/10.1016/j.ceramint.2013.09.080

electron–hole pairs. By coupling with Ag/AgX nanoparticles, the photocatalytic abilities of Ag/AgBr/TiO_2 [19,20], Ag/AgCl/TiO_2 [21], Ag/AgBr/BiOBr [22] were improved significantly. Wang et al. [19] prepared mesoporous TiO_2 coated with Ag and AgBr nanoparticles, which exhibited high photocatalytic activity for methyl orange degradation under visible light irradiation. Zhang et al. [20] synthesized Ag/AgBr/TiO_2 composites as a photoactive and durable catalyst toward the gas-phase degradation of benzene and acetone. Guo et al. [21] developed Ag/AgCl@TiO_2 composites for efficient photodegradation of 4-chlorophenol and photoreduction of Cr (VI) ion under visible light irradiation. However, Ag/AgBr nanoparticles modified ZnO as photocatalyst for dye degradation was scarcely reported.

In this paper, Ag/AgBr/ZnO nanocomposites have been successfully synthesized by two steps of deposition–precipitation method, and then followed by reduction under visible light irradiation. The photocatalytic activity and stability of the as-prepared Ag/AgBr/ZnO composites were evaluated by degrading the organic model pollutant of Rhodamine B (RhB) under visible light irradiation. Ag/AgBr/ZnO composites displayed much better photocatalytic activity than pure ZnO. Moreover, the as-prepared Ag/AgBr/ZnO composites exhibited good stability. The photocatalytic degradation efficiency after 10 recycles still kept at 70% of the first time activity. Therefore, the as-prepared Ag/AgBr/ZnO composites will be a promising highly active visible light-driven material for degrading dye.

2. Experimental

2.1. The preparation of Ag/AgBr/ZnO composites

First, AgBr/ZnO composites were prepared by the deposition–precipitation method. 1.0 g ZnO was added into 50 mL distilled water, and the suspension was sonicated for 10 min. Then, 1.2 g cetyltrimethylammonium bromide (CTAB) was added to the suspension, and the mixture was stirred for 60 min, then 0.21 g $AgNO_3$ in 1 mL NH_4OH (25 wt%) was dropped into the mixture. In this process, cationic surfactant CTAB was adsorbed onto the surface of ZnO to form the individual micelles which wrapped AgBr nanoparticles, limiting the numbers of nucleation sites for AgBr nanoparticles growing. After the resulting suspensions were stirred at room temperature for 12 h, the suspensions were filtered, washed with distilled water, and dried at 60 °C for 12 h. Finally, the powder was calcined in air at 500 °C for 3 h to obtain AgBr/ZnO composites. Then, the obtained sample was dispersed into distilled water and irradiated under visible light of the wavenumber of 400 nm to 800 nm by 300 W iodine tungsten lamp for 2 h while vigorous stirring. The color of the sample changed from light yellow to light gray, indicating that some Ag ions on the surface of AgBr/ZnO converted to Ag0 species. Thus, the Ag/AgBr/ZnO composites were obtained and named as Ag/AgBr/ZnO-2. Similarly, Ag/AgBr/ZnO-1 and Ag/AgBr/ZnO-3 were prepared with $AgNO_3$ of 0.11 g and 0.42 g, respectively. Additionally, Ag/AgBr/P25 composites were also prepared with commercial P25 instead of ZnO for comparison [20].

2.2. Material characterizations

The X-ray diffraction (XRD) measurement was carried out on Bruke D8 Advance X-ray powder diffractometer with Cu K_α radiation (40 kV, 40 mA) for phase identification. The morphology, particle sizes and chemical compositions of the products were examined by transmission electron microscopy (TEM, Tecnai G2 Spirit) equipped with an energy dispersion X-ray spectrometer (EDS). X-ray photoelectron spectroscopy (XPS) measurements were recorded on a PHI 5000C ESCA system with Al K_α radiation ($h\nu$ = 1486.6 eV). The UV–vis diffuse reflectance spectra (DRS) were measured by a Shimadzu UV-2500 spectrophotometer. The photoluminescence spectra (PL) were obtained by a Varian Cary Eclipse spectrometer with an excitation wavelength of 325 nm. The Brunauer–Emmett–Teller (BET) surface area and pore volume measurements were performed on a NOVA 2000 (Quantachrome, America) surface area analyzer with nitrogen as adsorbate. Samples were outgassed at 150 °C for 12 h prior to measurements.

2.3. Evaluation of photocatalytic performances

The photocatalytic performances of Ag/AgBr/ZnO composites were examined through degradation of RhB dye. The visible light was provided by 300 W iodine tungsten lamp at the wavenumber of 400 nm to 800 nm. 100 mg Ag/AgBr/ZnO composites were transferred into 100 mL 5 mg L^{-1} RhB aqueous solution. Then the dispersion was kept in dark for 30 min under magnetic stirring to reach the adsorption–desorption equilibrium. The distance between the surface of the suspension and the light source was about 50 cm. The illumination intensity on the suspension surface was ca. 4000 lx, measured by a lux meter. The RhB concentrations after irradiation for a definite time were estimated according to the absorbance at 552 nm measured by Shimadzu UV-2500 spectrophotometer. For comparison, the reactions were carried out in the presence of ZnO or Ag/AgBr/P25 and in the absence of any catalyst.

3. Results and discussions

3.1. Chemical composition, surface area and pore volume

Chemical composition, surface area and pore volume of Ag/AgBr/ZnO composites were determined by XPS and N_2 adsorption techniques. As shown in Table 1, the amounts of Ag and Br in the samples increased with the adding amounts of $AgNO_3$. However, the surface area and pore volume of Ag/AgBr/ZnO composites decreased slightly with the adding amounts of $AgNO_3$ increasing.

Table 1
Chemical composition, surface area and pore volume of Ag/AgBr/ZnO composites.

Sample	Ag wt %	Br wt %	Zn wt %	O wt %	Surface Area m^2/g	Pore Volume cm^3/g
Ag/AgBr/ZnO-1	7.11	4.79	70.70	17.40	4.21	0.0147
Ag/AgBr/ZnO-2	12.93	7.77	63.65	15.65	3.30	0.0131
Ag/AgBr/ZnO-3	16.50	10.05	58.94	14.51	2.86	0.0125

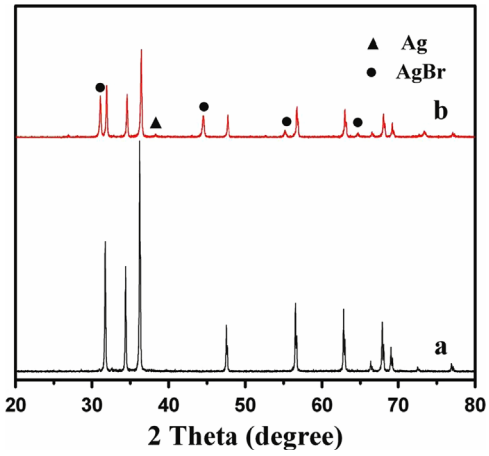

Fig. 1. XRD patterns of (a) pure ZnO and (b) Ag/AgBr/ZnO-2 composites.

3.2. XRD analysis

Fig. 1 shows the XRD patterns of pure ZnO and Ag/AgBr/ZnO-2 composites. The diffraction peaks at 2θ of 31.7°, 34.4°, 36.2°, 47.55°, 56.6° and 62.85° were respectively indexed to (100), (002), (101), (102), (110) and (103) diffraction planes of hexagonal structured ZnO (JCPDS card no. 076-0704). Apart from ZnO peaks, some new peaks at 31.1°, 44.4°, 55.1° and 64.6° corresponded to (200), (220), (222) and (400) diffraction planes of cubic phase AgBr (JCPDS card no.06-0438), and the peak at 38.1° characteristic of (111) diffraction of face-centered-cubic structured Ag (JCPDS card no. 04-0783) appeared in the Ag/AgBr/ZnO-2 composites. Hence, ZnO, Ag and AgBr existed in the Ag/AgBr/ZnO composites, no other impurity peaks were observed.

3.3. TEM analysis

Fig. 2 showed TEM images of pure ZnO and Ag/AgBr/ZnO-2 composites. Pure ZnO displayed nearly rod-like morphology and the surface of pure ZnO was smooth (Fig. 2A). In Ag/AgBr/ZnO composites, the surface of ZnO was attached by Ag/AgBr nanoparticles with small sizes of 5 nm in Fig. 2B. In addition, EDS result revealed the existence of Zn, O, Br and Ag, which were in agreement with XRD results.

3.4. XPS analysis

In the full XPS spectra of Ag/AgBr/ZnO-2 composites shown in Fig. 3A, strong peaks of Ag 3d, Br 3d, Zn 2p and

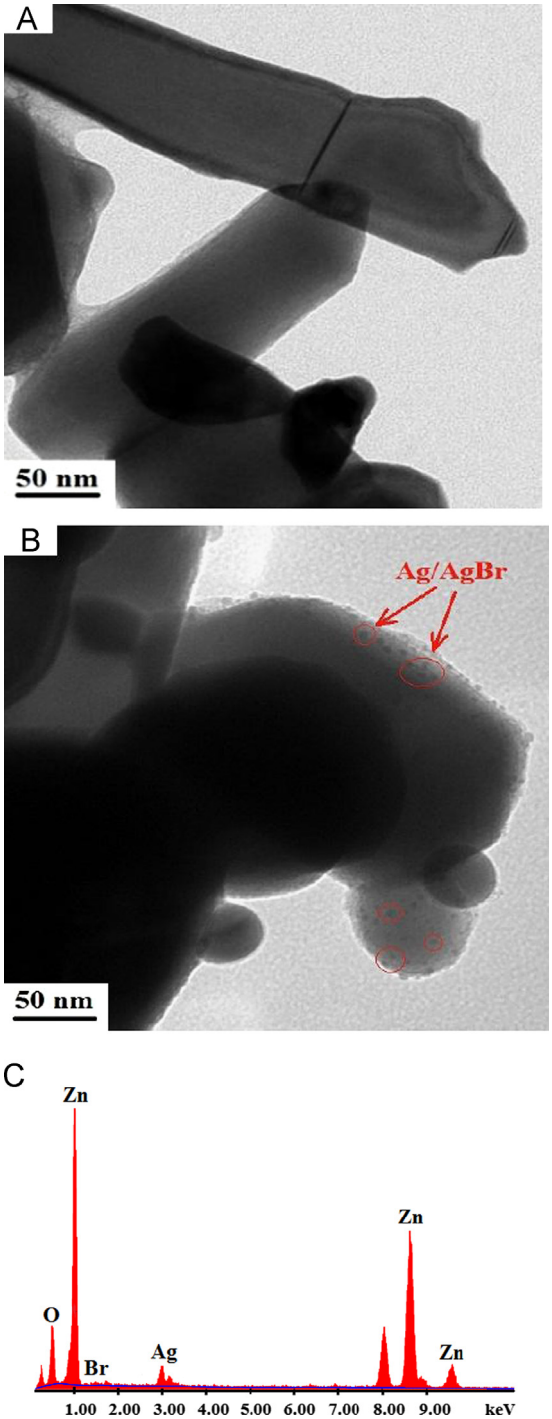

Fig. 2. TEM images of (A) pure ZnO, (B) Ag/AgBr/ZnO-2 composites and (C) EDS analysis for Ag/AgBr/ZnO-2 composites.

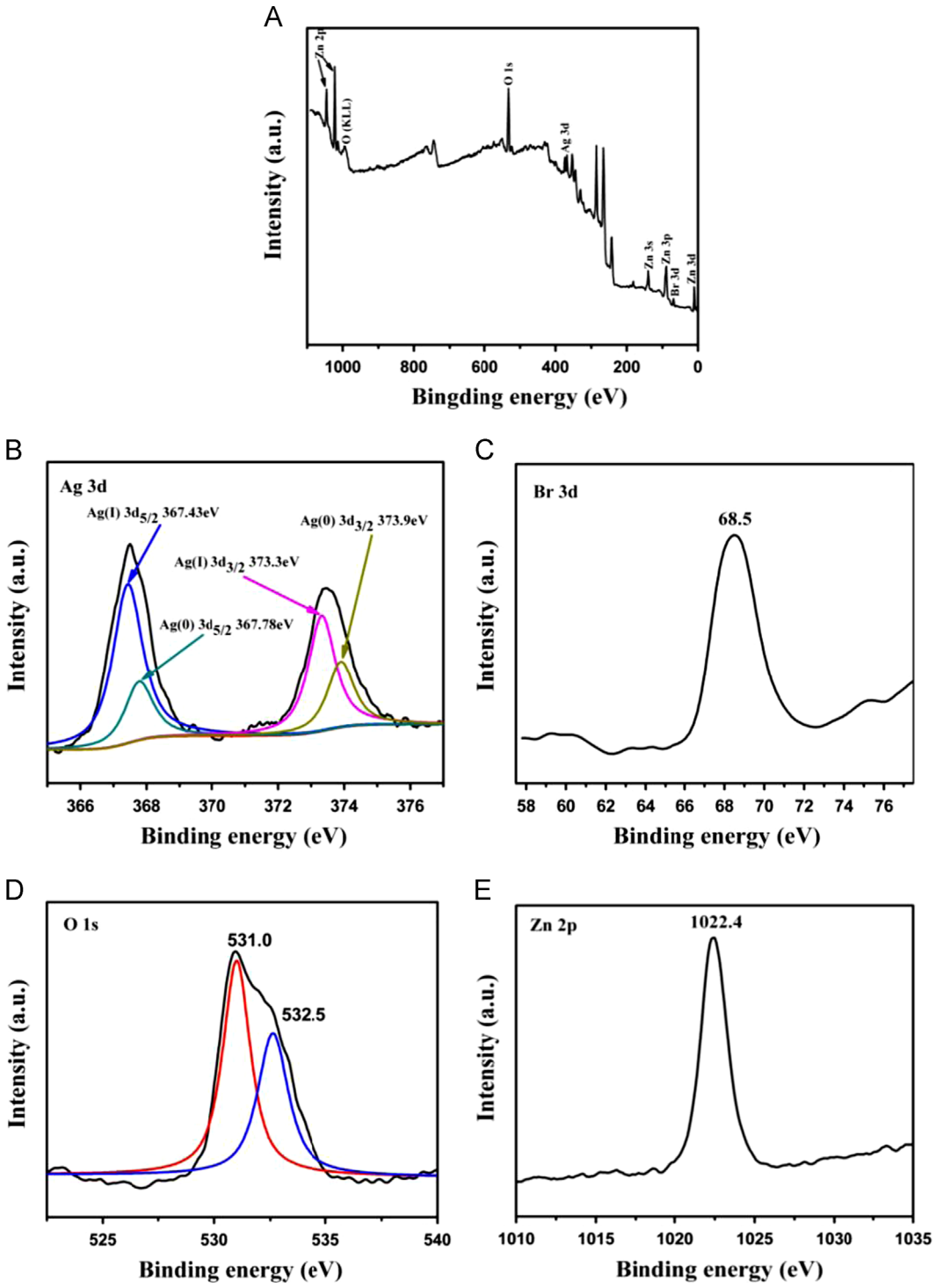

Fig. 3. XPS spectra of (A) full spectra of Ag/AgBr/ZnO-2 composites, (B) Ag 3d, (C) Br 3d, (D) O 1s, and (E) Zn 2p.

O 1s were observed. Peaks at 367.5 and 373.5 eV were assigned to Ag $3d_{5/2}$ and Ag $3d_{3/2}$ binding energies. The Ag $3d_{5/2}$ peak and Ag $3d_{3/2}$ peak could be further divided into two different peaks. The peaks at 367.43 eV and 373.3 eV were assigned to Ag (I) of AgBr, and the peaks at 367.78 eV and 373.9 eV were attributed to metallic Ag (0) [23]. The peak at 68.5 eV was ascribed to Br 3d in Fig. 3C. O 1s could be divided into two symmetrical peaks of 531.0 eV and 532.5 eV, which respectively corresponded to the lattice oxygen of ZnO and chemisorbed oxygen caused by the surface hydroxyl [24]. And the peak at 1022.4 eV was identified as Zn 2p of ZnO.

3.5. UV–vis diffuse reflectance

Fig. 4A shows the UV–vis diffuse reflectance spectra of pure ZnO and Ag/AgBr/ZnO-2 composites. It is noticeable that the loadings of Ag/AgBr onto ZnO support significantly

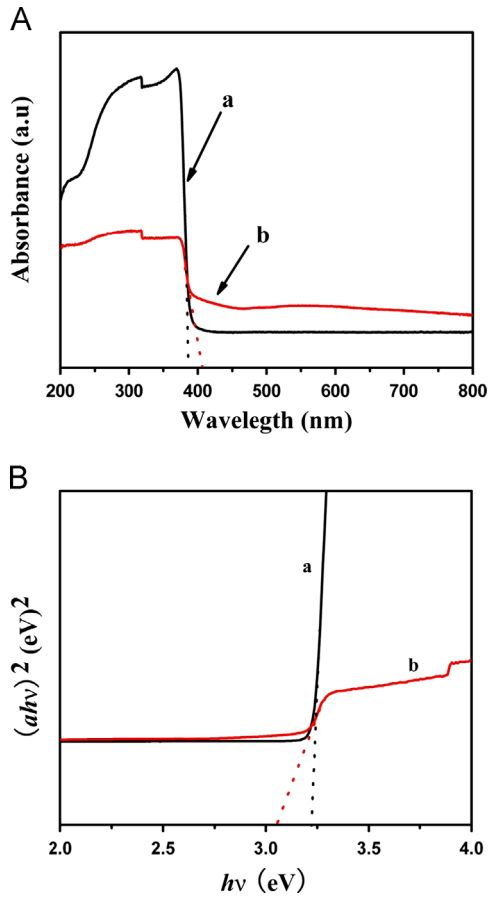

Fig. 4. (A) DRS spectra and (B) Plots of $(\alpha h\nu)^2$ versus energy ($h\nu$) for the band gap energy of (a) pure ZnO and (b) Ag/AgBr/ZnO-2 composites.

affected the optical property of ZnO. Ag/AgBr/ZnO-2 composites possessed the stronger absorption in the visible light range compared with pure ZnO, which was resulted from the surface plasmon absorption of Ag nanoparticles and light absorption of AgBr nanoparticles. Ag/AgBr/ZnO-2 showed absorption edge at about 406 nm, while an absorption edge of ZnO was at around 385 nm.

The band gap energy of a semiconductor can be calculated by the following formula [25]:

$$\alpha h\nu = A(h\nu - E_g)^{n/2} \quad (1)$$

where α, h, ν, E_g and A are absorption coefficient, Planck constant, light frequency, band gap energy, and a constant, respectively. For Ag/AgBr/ZnO composites, the value of n is 4, because n is determined by the type of optical transition of a semiconductor (i.e. $n=1$ for direct transition and $n=4$ for indirect transition). Therefore, E_g of ZnO was calculated to be 3.22 eV, and the band gap E_g of Ag/AgBr/ZnO-2 was narrowed to 3.06 eV. The narrowed band gap favored the photocatalytic performance of Ag/AgBr/ZnO composites during the visible light region.

3.6. Photocatalytic activity of degrading RhB

Fig. 5A shows the photocatalytic activities over pure ZnO, Ag/AgBr/ZnO and Ag/AgBr/P25 composites. The degradation

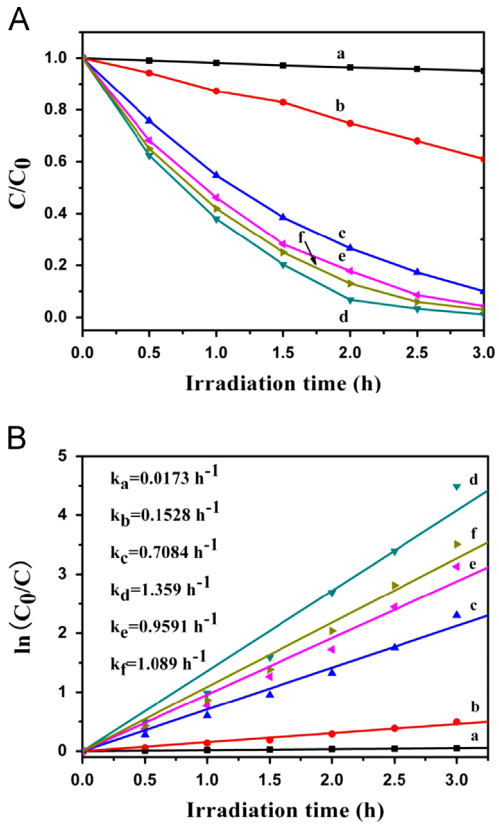

Fig. 5. (A) Photodegradation activities and (B) First-order kinetic plots for the photodegradation of RhB over (a) blank, (b) pure ZnO, (c) Ag/AgBr/ZnO-1, (d) Ag/AgBr/ZnO-2, (e) Ag/AgBr/ZnO-3 and (f) Ag/AgBr/P25.

of RhB hardly occurred without any catalyst, which suggested that the photoinduced self-sensitized photolysis of RhB could be neglected. The degradation efficiency of RhB solution over pure ZnO was about 38% in 3 h. However, the degradation efficiency was significantly improved under the same condition after loaded by Ag/AgBr nanoparticles. The photocatalytic efficiencies of Ag/AgBr/ZnO-1 and Ag/AgBr/ZnO-3 were enhanced to 90% and 95%, respectively. Noticeably, Ag/AgBr/ZnO-2 gave the highest degradation efficiency, almost 100% RhB was degraded within 3 h, which was slightly higher than that of Ag/AgBr/P25. To have a better understanding of the reaction kinetics of the RhB degradation catalyzed by various samples, Fig. 5B shows the relationships between ln (C_0/C) and the irradiation time for RhB degradation. As the relationships were linear ($R \geq 0.99$), the photocatalytic degradation curves fit well with first-order reaction. The Ag/AgBr/ZnO-2 composites exhibited the highest rate constant ($k=1.359\ h^{-1}$) in all of samples, which was approximately 8.5 times larger than that of pure ZnO ($k=0.1528\ h^{-1}$), even larger than that of as-prepared Ag/AgBr/P25 catalyst ($k=1.089\ h^{-1}$).

3.7. Photocatalytic stability

Photocatalyst stability is an important factor for its practical application. The circulating runs in the photodegradation of RhB over Ag/AgBr/ZnO-2 composites were conducted, as

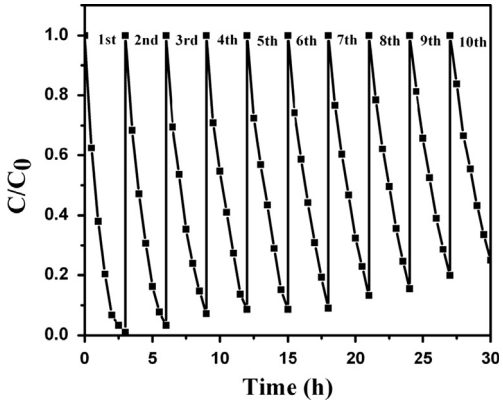

Fig. 6. Circulating runs in the photodegradation of RhB over Ag/AgBr/ZnO-2 composites.

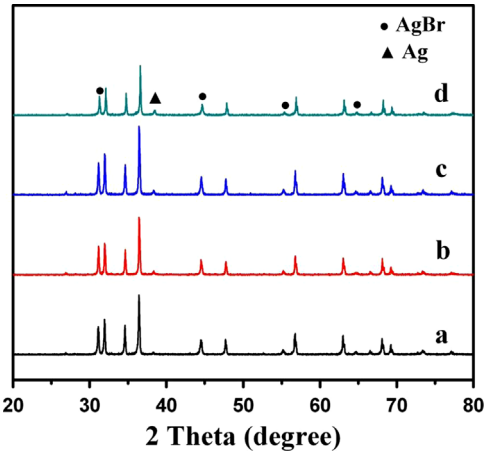

Fig. 7. XRD patterns of Ag/AgBr/ZnO-2 composites before and after reuses for the photocatalytic degradation of RhB, (a) fresh sample, (b) after 3 recycles, (c) 5 recycles and (d) 10 recycles.

shown in Fig. 6. The photocatalytic activities of Ag/AgBr/ZnO-2 composites slightly decreased with the recycle times, but photodegradation efficiency still kept at 70% of fresh catalyst after the 10th run, indicating its stability.

Fig. 7 shows the XRD patterns of Ag/AgBr/ZnO-2 composites before and after degradation of RhB. After several catalytic runs, the peak positions are the same as those of the fresh catalyst. However, the ratios of the peaks intensities changed slightly. The intensity of metal Ag became stronger with the recycle times increasing, while the AgBr peaks became weaker, suggesting that AgBr gradually changed into more Ag^0 during the photodegration processes. The changes in chemical state of Ag species were possibly resulted from the combination of photogenerated electrons with Ag^+ to form Ag, which made the amounts of Ag gradually increase during photocatalytic reactions. Similar phenomena were also reported in Ag/AgBr and AgBr/TiO_2 catalysts [17,26].

3.8. Possible photocatalytic mechanism

To ascertain the main reactive species for the degradation of RhB, the addition effects of radical scavengers were examined

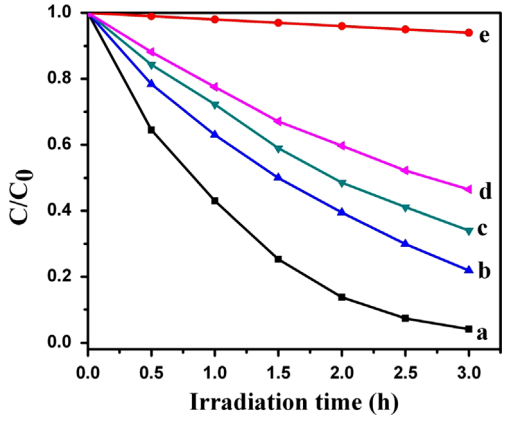

Fig. 8. Effects of adding different radical scavengers on the degradation of RhB over Ag/AgBr/ZnO-2 catalyst (a) no scavenger, (b) with 1 mM EDTA, (c) with 10 mM methanol, (d) with 5 mM DMSO, and (e) with 1 mM p-benzoquinone.

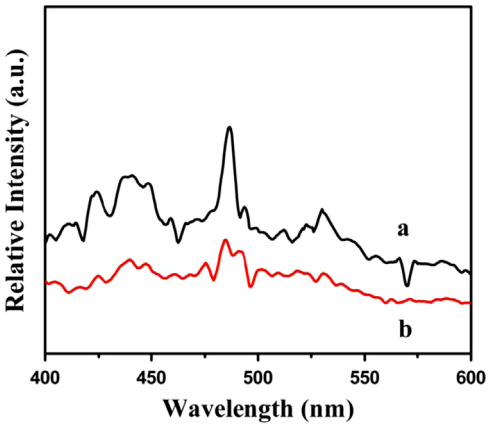

Fig. 9. Photoluminescence spectra of (a) ZnO and (b) Ag/AgBr/ZnO-2 composites.

in order to discuss the reaction mechanism (Fig. 8). Here, methanol was used to quench the •OH in the solution [27], ethylene diamine tetraacetic acid (EDTA) for h^+ scavenger [28], p-benzoquinone for $•O_2^-$ quencher [29], and dimethyl sulfoxide (DMSO) for e^- scavenger [19]. Fig. 8 shows the photocatalytic degradation curves over Ag/AgBr/ZnO-2 composites in the presence of different scavengers. The additions of methanol, EDTA and DMSO led to much decreases in degradation activities, which implied that •OH, h^+ and e^- were the active reactive species. The additions of p-benzoquinone made the degradation of RhB almost inhibit, suggesting that $•O_2^-$ was the main reactive species. Moreover, Huang et al. [30] and Geng et al. [31] have reported that the generated h^+ on AgBr could oxidize Br^- to Br^0, and Br^0 further oxidized RhB dye as reactive species.

Since photoluminescence spectrum emission arises from the recombination of excited electrons and holes, the PL technique is useful for disclosing the migration, transfer, and recombination processes of the photogenerated electron–hole pairs in the semiconductors. Fig. 9 shows the PL spectra of ZnO and Ag/AgBr/ZnO-2 with the excitation wavelength of 325 nm.

Pure ZnO showed higher intensity of emission spectrum than that of Ag/AgBr/ZnO-2, which suggested the photogenerated electrons and holes might recombine rapidly in ZnO system. As we know, a weaker PL intensity represents a lower recombination probability of the electron–hole under light irradiation. In Ag/AgBr/ZnO system, due to the presence of Ag/AgBr nanoparticles, photogenerated electrons easily transferred from AgBr to ZnO, in addition, noble metal Ag also trapped photogenerated electrons because of the Schottky barrier [12]. Hence, the electron–hole recombination rates were greatly decreased, thus leading to the improved photocatalytic activity.

Possible reaction mechanism over Ag/AgBr/ZnO under visible light irradiation was proposed in Fig. 10. During the photocatalytic oxidation process, AgBr could be excited to form photogenerated electron–hole pairs under visible light irradiation. Subsequently, the photogenerated electrons transferred from the conduction band (CB) of AgBr to that of ZnO or trapped by Ag on AgBr nanoparticles. These electrons further reacted with O_2 adsorbed on the surface of catalyst to generate active $\bullet O_2^-$. At the same time, h^+ in the valence band (VB) of AgBr and ZnO combined with H_2O to produce active $\bullet OH$. Additionally, reactive holes on the VB of AgBr could oxidize Br^- ions to Br^0 which were the reactive species for degrading RhB dye. These reactive radical species of $\bullet O_2^-$, $\bullet OH$, h^+, e^- and Br^0 were so reactive that they could efficiently degrade RhB into less organic matters and finally into H_2O and CO_2. In the photocatalytic reaction process, recombinations of the electrons and holes were efficiently prevented, resulting in enhanced photocatalytic activity of Ag/AgBr/ZnO composites.

According to the previous reports [32–34], the possible degradation pathways of RhB were shown in Fig. 11. The photodegradation of RhB includes four main processes: N-deethylation, chromophore cleavage, opening-ring and mineralization. During the photocatalytic oxidation process, various active intermediate species including $\bullet O_2^-$, $\bullet OH$, h^+, e^- and

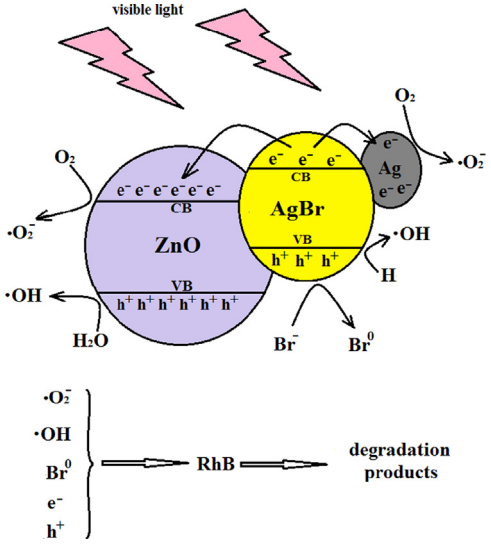

Fig. 10. Possible reaction mechanism over Ag/AgBr/ZnO composites under visible light irradiation.

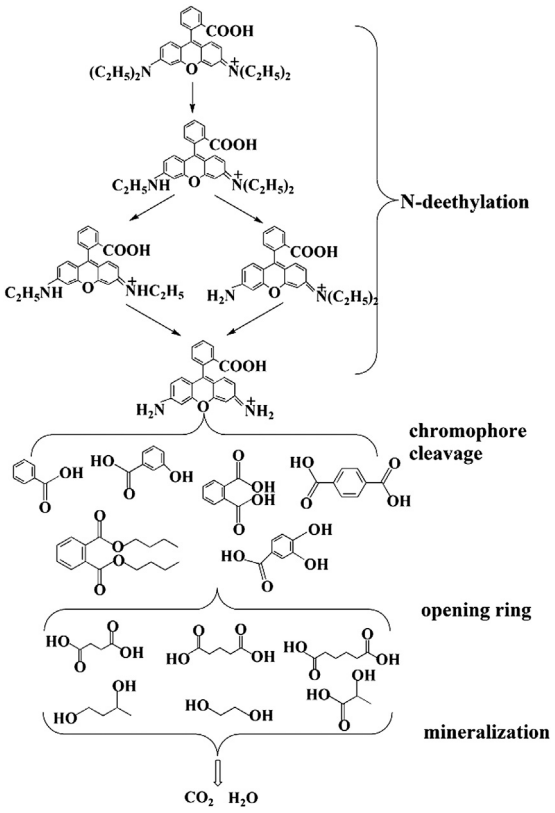

Fig. 11. Possible degradation pathway of RhB over Ag/AgBr/ZnO composites.

Br^0 were formed, which were involved in destruction process of RhB structure. Their oxidation or reduction activities made RhB N-deethylated and destruct the conjugated structure. With the prolonged time of light irradiation, the effects of active intermediate species were enhanced, resulting in further opening-ring and mineralization of less organic matters.

4. Conclusions

Ag/AgBr/ZnO composites were successfully synthesized by two steps of deposition–precipitation method, and then followed by reduction under visible light irradiation. Because of the presence of small sized Ag/AgBr nanoparticles on ZnO surface, Ag/AgBr/ZnO composites possessed strong absorption in the visible light range and excellent performances for the degradation of RhB compared with pure ZnO and Ag/AgBr/P25 samples. Moreover, through catalytic repetitive tests, Ag/AgBr/ZnO composites remained excellent stability and regeneration capability, although some AgBr were converted to more Ag during the photocatalytic processes. The enhanced photocatalytic activity was due to the synergistic effects coming from effective separation of photogenerated e^-–h^+, narrowed band gap and enhanced visible light absorption because of the modified Ag/AgBr. Thus, Ag/AgBr/ZnO composites may be a promising efficient photocatalyst for pollutants abatement.

Acknowledgments

We sincerely acknowledge the financial supports from the National Natural Science Foundation of China (21073049 and 21373069), New Century Excellent Talents in University (NCET-10-0064), State Key Lab of Urban Water Resource and Environment of Harbin Institute of Technology (HIT2013TS01) and Open Fund from Key Laboratory of Functional Inorganic Material Chemistry (Heilongjiang University) Ministry of Education.

References

[1] T. Wang, L. Liang, R. Wang, Y. Jiang, K. Lin, J. Sun, Magnetic mesoporous carbon for efficient removal of organic pollutants, Adsorption 18 (2012) 439–444.
[2] J. Mansouri, S. Harrisson, V. Chen, Strategies for controlling biofouling in membrane filtration systems: challenges and opportunities, Journal of Materials Chemistry A 20 (2010) 4567–4586.
[3] T. Zhang, L. Ding, H. Ren, X. Xiong, Ammonium nitrogen removal from coking wastewater by chemical precipitation recycle technology, Water Research 43 (2009) 5209–5215.
[4] T. Yazawa, F. Machida, K. Oki, A. Mineshige, M. Kobune, Novel porous TiO_2 glass–ceramics with highly photocatalytic ability, Ceramics International 35 (2009) 1693–1697.
[5] S. Chakrabarti, B.K. Dutta, Photocatalytic degradation of model textile dyes in wastewater using ZnO as semiconductor catalyst, Journal of Hazardous Materials 112 (2004) 269–278.
[6] Y. Dong, K. He, L. Yin, A. Zhang, A facile route to controlled synthesis of Co_3O_4 nanoparticles and their environmental catalytic properties, Nanotechnology 18 (2007) 435602–435607.
[7] J. Li, F. Sun, K. Gu, T. Wu, W. Zhai, W. Li, S. Huang, Preparation of spindly CuO micro-particles for photodegradation of dye pollutants under a halogen tungsten lamp, Applied Catalysis A: General 406 (2011) 51–58.
[8] F. Yang, N. Yan, S. Huang, Q. Sun, L. Zhang, Y. Yu, Zn-doped CdS nanoarchitectures prepared by hydrothermal synthesis: mechanism for enhanced photocatalytic activity and stability under visible light, Journal of Physical Chemistry C 116 (2012) 9078–9084.
[9] E.S. Jang, J.H. Won, S.J. Hwang, J.H. Choy, Fine tuning of the face orientation of ZnO crystals to optimize their photocatalytic activity, Advanced Materials 18 (2006) 3309–3312.
[10] P. Jongnavakit, P. Amornpitoksuk, S. Suwanboon, N. Ndiege, Preparation and photocatalytic activity of Cu-doped ZnO thin films prepared by the sol–gel method, Applied Surface Science 258 (2012) 8192–8198.
[11] H. Qin, W. Li, Y. Xia, T. He, Photocatalytic activity of heterostructures based on ZnO and N-doped ZnO, ACS Applied Materials and Interfaces 3 (2011) 3152–3156.
[12] Z.Z. Han, L.L. Ren, Z.H. Cui, C.Q. Chen, H.B. Pan, J.Z. Chen, Ag/ZnO flower heterostructures as a visible-light driven photocatalyst via surface Plasmon resonance, Applied Catalysis B: Environmental 126 (2012) 298–305.
[13] S. Lam, J. Sin, A.Z. Abdullah, A.R. Mohamed, ZnO nanorods surface-decorated by WO_3 nanoparticles for photocatalytic degradation of endocrine disruptors under a compact fluorescent lamp, Ceramics International 39 (2013) 2343–2352.
[14] K. Vignesh, A. Suganthi, M. Rajarajan, S.A. Sara, Photocatalytic activity of AgI sensitized ZnO nanoparticles under visible light irradiation, Power Technology 224 (2012) 331–337.
[15] V. Eskizeybek, F. Sarı, H. Gülce, A. Gülce, A. Avcı, Preparation of the new polyaniline/ZnO nanocomposite and its photocatalytic activity for degradation of methylene blue and malachite green dyes under UV and natural sun lights irradiations, Applied Catalysis B: Environmental 119–120 (2012) 197–206.
[16] Y. Zhu, H. Liu, L. Yang, J. Liu, Study on the synthesis of Ag/AgCl nanoparticles and their photocatalytic properties, Materials Research Bulletin 47 (2012) 3452–3458.
[17] D. Wang, Y. Duan, Q. Luo, X. Li, L. Bao, Visible light photocatalytic activities of plasmonic Ag/AgBr particles synthesized by a double jet method, Desalination 270 (2011) 174–180.
[18] W. Cui, H. Wang, Y. Liang, L. Liu, B. Han, Preparation of Ag@AgI-intercalated $K_4Nb_6O_{17}$ composite and enhanced photocatalytic degradation of Rhodamine B under visible light, Catalysis Communications 36 (2013) 71–74.
[19] D. Wang, Y. Duan, Q. Luo, X. Li, J. An, L. Bao, L. Shi, Novel preparation method for a new visible light photocatalyst: mesoporous TiO_2 supported Ag/AgBr, Journal of Materials Chemistry A 22 (2012) 4847–4854.
[20] Y. Zhang, Z. Tang, X. Fu, Y. Xu, Nanocomposite of Ag–AgBr–TiO_2 as a photoactive and durable catalyst for degradation of volatile organic compounds in the gas phase, Applied Catalysis B: Environmental 106 (2011) 445–452.
[21] J. Guo, B. Ma, A. Yin, K. Fan, W. Dai, Highly stable and efficient Ag/AgCl@TiO_2 photocatalyst: preparation, characterization, and application in the treatment of aqueous hazardous pollutants, Journal of Hazardous Materials 211–212 (2012) 77–82.
[22] H. Cheng, B. Huang, P. Wang, Z. Wang, Z. Lou, J. Wang, X. Qin, X. Zhang, Y. Dai, In situ ion exchange synthesis of the novel Ag/AgBr/BiOBr hybrid with highly efficient decontamination of pollutants, Chemical Communications 47 (2011) 7054–7056.
[23] P. Wang, B. Huang, X. Qin, X. Zhang, Y. Dai, M. Whangbo, Ag/AgBr/$WO_3 \cdot H_2O$: visible-Light photocatalyst for bacteria destruction, Inorganic Chemistry 48 (2009) 10697–10702.
[24] N.S. Ramgir, I.S. Mulla, V.K Pillai, Micropencils and microhexagonal cones of ZnO, Journal of Physical Chemistry B 110 (2006) 3995–4001.
[25] J. Cao, B. Luo, H. Lin, S. Chen, Synthesis, characterization and photocatalytic activity of AgBr/H_2WO_4 composite photocatalyst, Journal of Molecular Catalysis A: Chemical 344 (2011) 138–144.
[26] Y.J. Zang, R. Farnood, Photocatalytic activity of AgBr/TiO_2 in water under simulated sunlight irradiation, Applied Catalysis B: Environmental 79 (2008) 334–340.
[27] R. Dong, B. Tian, J. Zhang, T. Wang, Q. Tao, S. Bao, F. Yang, C. Zeng, AgBr@Ag/TiO_2 core–shell composite with excellent visible light photocatalytic activity and hydrothermal stability, Catalysis Communications. 38 (2013) 16–20.
[28] D. Wang, L. Shi, Q. Luo, X. Li, J. An, An efficient visible light photocatalyst prepared from TiO_2 and polyvinyl chloride, Journal of Materials Science 47 (2012) 2136–2145.
[29] C. Hu, T.W. Peng, X.X. Hu, Y.L. Nie, X.F. Zhou, J.H. Qu, H. He, Plasmon-induced photodegradation of toxic pollutants with Ag–AgI/Al_2O_3 under visible-light irradiation, Journal of the American Chemical Society 132 (2010) 857–862.
[30] P. Wang, B. Huang, X. Zhang, X. Qin, H. Jin, Y. Dai, Z. Wang, J. Wei, J. Zhan, S. Wang, J. Wang, M. Wangbo, Highly efficient visible-light plasmonic photocatalyst Ag@AgBr, Chemistry A European Journal 15 (2009) 1821–1824.
[31] L. Kuai, B.Y. Geng, X.T. Chen, Y.Y. Zhao, Y.C. Luo, Facile subsequently light-induced route to highly efficient and stable sunlight-driven Ag–AgBr plasmonic photocatalyst, Langmuir 26 (2010) 18723–18727.
[32] Z. He, C. Sun, S. Yang, Y. Ding, H. He, Z. Wang, Photocatalytic degradation of rhodamine B by Bi_2WO_6 with electron accepting agent under microwave irradiation: mechanism and pathway, Journal of Hazardous Materials 162 (2009) 1477–1486.
[33] T.S. Natarajan, K. Natarajan, H.C. Bajaj, R.J. Tayade, Enhanced photocatalytic activity of bismuth-doped TiO_2 nanotubes under direct sunlight irradiation for degradation of Rhodamine B dye, Journal of Nanoparticle Research 15 (2013) 1669–1687.
[34] N.U. Silva, T.G. Nunes, M.S. Saraiva, M.S. Shalamzari, P.D. Vaz, O. C. Monteiro, C.D. Nunes, Photocatalytic degradation of rhodamine B using Mo heterogeneous catalysts under aerobic conditions, Applied Catalysis B: Environmental 113–114 (2012) 180–191.